Intelligent Vehicle Counting and Classification Sensor for Real-Time Traffic Surveillance

Article *in* IEEE Transactions on Intelligent Transportation Systems · September 2017

DOI: 10.1109/TITS.2017.2741507

CITATIONS
150

READS
4,033

3 authors:

Walid Balid
Panduit
69 PUBLICATIONS **651** CITATIONS
SEE PROFILE

Hasan Tafish
University of Oklahoma
9 PUBLICATIONS **317** CITATIONS
SEE PROFILE

Hazem Refai
University of Oklahoma
265 PUBLICATIONS **3,266** CITATIONS
SEE PROFILE

Intelligent Vehicle Counting and Classification Sensor for Real-Time Traffic Surveillance

Walid Balid, *Member, IEEE*, Hasan Tafish, and Hazem H. Refai, *Member, IEEE*

***Abstract*—Real-time traffic surveillance is essential in today's intelligent transportation systems and will surely play a vital role in tomorrow's smart cities. The work detailed in this paper reports on the development and implementation of a novel smart wireless sensor for traffic monitoring. Computationally efficient and reliable algorithms for vehicle detection, speed and length estimation, classification, and time-synchronization were fully developed, integrated, and evaluated. Comprehensive system evaluation and extensive data analysis were performed to tune and validate the system for a reliable and robust operation. Several field studies conducted on highway and urban roads for different scenarios and under various traffic conditions resulted in 99.98% detection accuracy, 97.11% speed estimation accuracy, and 97% length-based vehicle classification accuracy. The developed system is portable, reliable, and cost-effective. The system can also be used for short-term or long-term installment on surface of highway, roadway, and roadside. Implementation cost of a single node including enclosure is US $50.**

***Index Terms*—Intelligent Transportation System (ITS), WSN, Magnetometer Sensors, Vehicles Detection and Classification, Traffic Surveillance, Smart Cities**

I. Introduction

TRAFFIC surveillance is an integral part of the intelligent transportation system (ITS) network. Providing a reliable, real-time traffic monitoring has a major influence on the efficiency and safety of highways and roadways. Increasing demand on surface transportation—driven by an ever-growing population—and its impact on traffic safety has been a major concern for transportation agencies. The U.S. federal highway administration (FHWA) predicts a 23% increase in vehicle miles traveled by 2032 (i.e., 1.04% annual growth) [1].

Statistical studies by the World Health Organization (WHO) reported 1.25 million people die and up to 50 million injuries occur every year on the world's roads [2]. The U.S. National Highway Traffic Safety Administration (NHTSA) reported 32,719 fatalities and 2.313 million injuries in 2013, 28% of which are speed-related [3]. Annual traffic fatalities caused by trucks reportedly cause 4,000 deaths and 100,000 injuries to travelers. Vehicular fatalities on U.S. roadways have an annual direct economic cost of $242 billion, resulting from 24 million crashes. This figure represents 1.6% of the $14.96 trillion U.S. Gross Domestic Product (GDP) reported in 2010 [4]. This total increases to $836 billion when considering societal harm from vehicle crashes. Furthermore, 44% of the U.S. roadways are congested. According to the 2015 Urban Mobility Scorecard report [5], traffic congestion costs $160 billion each year in the U.S. as a result of seven billion lost hours and three billion gallons fuel wasted. Additionally, 31% of CO2 emissions come from vehicles tailpipes [6].

Without assertive, proactive solutions, traffic crashes are predicted to rise, and roadways congestion is estimated to worsen. The annual delay in the U.S. will grow to 8.3 billion hours, resulting in an increasing cost of $192 billion [5].

Although vehicle travel on U.S. highways increased by 39% from 1990 to 2013, new road mileage increased by only 4%. Hence, to mitigate the impact of continued growing demand on transportation and to prevent worsening levels of roadways congestion, it has been suggested that the U.S. FHWA would be required to expand current transportation infrastructure capacity by 23%. One option to achieve this goal is adding 4,200 miles of new roadway each year [7]. Another option is developing technologies that maximize existing transportation infrastructure capacity and improve efficiency, making transportation systems safe, efficient, and more reliable for the rapidly approaching era of smart cities. One essential requirement for needed ITSs is the reliable and real-time execution and data exchange among various ITS infrastructure components to facilitate instantaneous decision-making.

Vehicle detection and traffic surveillance technologies are a core component of ITS. Current technologies can be classified into three types of sensors: 1) Intrusive, 2) Non-intrusive, and 3) Off-roadway. Intrusive sensors include magnetic detectors, pneumatic road tubes, piezoelectric, and inductive loop (IDL) that are embedded in the road surface using a saw-cut or hole. Non-intrusive sensors include vision systems, microwave radar, and infrared and ultrasonic detectors in which sensors are mounted overhead on roadways or roadsides. Off-roadway sensors are mobile sensors that enable sensing via aircraft or satellite, as well as probe vehicles equipped with Global Positioning System (GPS) receiver. A detailed description of these technologies can be found in [7], [8].

Intrusive sensors are large, expensive, power-hungry, and require lane closure and traffic disruption for installation or regular maintenance. Additionally, these sensors rely on pavement geometry, meaning that a deterioration in pavement will result unreliable data. Moreover, resurfacing or repairing roadways require reinstalling the sensors. Worker safety for those deploying intrusive system has been a concern.

Manuscript received ---------- xx, xxxx; revised ---------- xx, xxxx; accepted ---------- xx, xxxx. Date of publication ---------- xx, xxxx; date of current version ---------- xx, xxxx;. This work has been supported by the U.S. Department of Transportation in Oklahoma under Grant ODOT SPR ITEM NUMBER 2250.

Walid Balid, Hasan Tafish, and Hazem H. Refai are with the University of Oklahoma, Graduate College, Electrical and Computer Engineering Department, OK 74135 USA (e-mail: walid@ou.edu; hasan.tafish@ou.edu, hazem@ou.edu).

Although vision and radar systems are widely considered accurate and typically do not disrupt traffic, performance is effected by weather conditions. Off-roadway sensors provide limited traffic statistics at fixed location, as well as limited coverage dependent upon the number of probe vehicle [7], [8]. The high cost associated with the aforementioned technologies limits the special distribution and large-scale integration of these sensors, and they work independently of each other. The scalability and availability of traffic monitoring systems are essential for efficient and reliable, real-time ITSs [9].

Inexpensive, nonintrusive, portable, and easy-to-install technologies are critically needed to supplement current ITS. Magnetometer (MAG) sensors have been found to serve as an alternative to IDLs. They are sensitive, inexpensive, and immune to weather conditions or environmental factors [10]. Wireless sensor networks (WSN) are emerging and a key enabler for enormous number of sensing applications. WSNs have demonstrated exceptional features, such as flexibility, scalability, reliability, and power efficiency [11]. Integrating MAG and WSN has enabled autonomous methods for real-time traffic surveillance application, such as vehicle detection on roadways [12]–[15], vehicle detection in parking lots [16]–[18], speed estimation [19]–[28], and vehicle classification [19], [29]–[34]. Many credit the PATH program at University of California [8] for initiating the use of MAG sensors in traffic monitoring applications.

The essential principle in the MAG method is recognizing that vehicles have a large mass of highly-permeable ferrous materials (e.g., nickel, iron, steel) that cause local disturbance in the Earth's magnetic field flux lines. As vehicles pass through this magnetic field, magnetic flux lines are absorbed in a non-uniform manner and creates a non-uniformity in flux lines, as shown in Fig. 1. Disturbance magnitude and direction depends on several factors, including speed, size, density, and permeability of vehicle structure. Disturbance represents vehicle magnetic signature (VMS), which can be sampled via passive magnetic sensors (i.e., MAG).

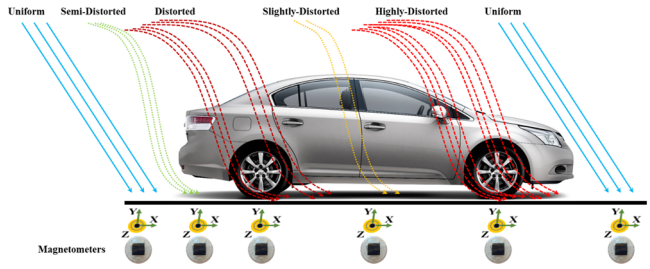

Fig. 1. Earth's magnetic field lines distorted by passing vehicle

A. Contributions

This paper describes a complete hardware design, computational algorithms development, real world extended field deployments, extensive and comprehensive testing, and large-scale evaluation of a non-intrusive, inexpensive, and portable intelligent vehicle counting and classification sensor (*i*VCCS). The sensor integrates state-of-the-art embedded components, managed by distinctive algorithms for the implementation of various traffic monitoring applications. The sensor can accurately detect, count, estimate speed and length, and classify vehicles in real-time. *i*VCCS is similar to Sensys [35] in concept, but differ in practice including cost, installation, real-time data accessibility, design and algorithm availability. *i*VCCS could be easily integrated in a comprehensive IoT framework, given its aforementioned characteristics. Furthermore, unlike commercially available solutions [35], *i*VCCS is installed on atop of roadways or roadside which required development of specific algorithms to counteract for physical contacts. The paper also identifies real field disturbance factors that influence the accuracy of vehicle detection and implements calibration algorithms to successfully compensate for their impacts. All design aspects and implementations are addressed including the repeatability of VMS and the consistency of MAG sensor output.

The balance of this paper is organized as follows. Related works is presented in Section II. A description of *i*VCCS system is provided in Section III. Algorithms development and system integration are discussed in Section IV. A field study and data analysis are reported in Section V. Further research and conclusion are provided in Section VI.

II. Earlier Studies

Recently, several studies have been published about traffic surveillance using MAG sensors. For example, authors in [36] proposed a 2-axis MAG for detecting vehicle driving direction. A high detection rate of 99% was observed when traveling vehicles pass closely to the sensor. Performance degraded to 89% as the signal-to-noise ratio (SNR) decreased. A two-threshold, four-state machine algorithm was introduced in [12] for vehicle detection using 3-axis MAG. Authors in [13] proposed a short-time transform detection and recognition algorithm using a MAG sampled at 2KHz. A 3-axis MAG was used in [16] used for vehicle detection in parking lots. In [17], a street parking system using a MAG was introduced, and in [18], researchers proposed a vehicle parking detection method using a normalized cross-correlation of a 3-axis MAG signal. Authors in [37] proposed a scheme for identifying the heading direction of a moving vehicle using a 2-axis MAG.

A speed estimation algorithm using magnetic sensors was proposed in [19]–[21]. In these studies, a cross-correlation factor R is calculated via FFT by a master node from raw data received from two roadside sensor nodes. Time delay is obtained by R when the resulting signal is maximized. Although this method achieved relatively accurate estimates, it proved computationally expensive. A region-based speed estimation is proposed in [22]. In this work, the first order derivative is calculated on each sensor node, and a region of each signal is selected based on a threshold sent to the server for processing. Study [23] claims 90% average speed estimation accuracy by analyzing magnetic length using a single roadside node composed of an accelerometer and MAG. Two magnetic sensor nodes are used in [24] to estimate speed, and a third node is used for data fusion. Actual speed was under-estimated at an error rate of 20%. Authors in [25] proposed using four MAG nodes per lane—two on each side of the lane. A 10% error in speed estimation under low speed test (e.g., 6–13m/s) was reported. Studies in [26], [27]

proposed algorithms for speed estimation using a single MAG. Notably, this method was designed to estimate average speed only for the number of passing vehicles over time.

Four roadside MAG nodes were used in [19] for detection, speed estimation, and vehicle classification into four groups based on length and height ratio. Acceptable accuracy was reported. However, the proposed method works for only single lane urban roads. Furthermore, the major dataset was composed of small vehicles records; only a few trucks were included. Thus, results would prove inconclusive. Vehicle classification and detection using an improved support vector machine classifier was proposed in [29], using a single-axis MAG. The proposed algorithm uses concavity and convexity of magnetic signatures to distinguish among heavy tracked, tracked, and light-wheeled vehicles. A limited dataset of 93 vehicles resulted in 90% classification accuracy. In [31], a 3-axis MAG was used for a detection and classification in low-speed congested traffic. A fixed-threshold state machine algorithm was employed for vehicle detection, and a tree-based algorithm was implemented for classification. Vehicles were divided into four-groups, namely motorcycles, saloon, buses, and SUVs. Five features were extracted to distinguish between the groups, namely the duration, energy, average energy of vehicle signature, and ratio of positive to negative energy on both X and Y axis. The dataset included only 253 vehicles. Although high detection and classification rates were reported, the dataset was limited to a small number of samples, and trucks and pickups were not considered. Authors in [33] proposed a vehicle classification system using two nodes installed on roadside, each combining an accelerometer and MAG. Three features, namely the integral of each of MAG magnitude, accelerometer magnitude and magnitude distribution, were extracted and normalized to vehicle speed. Several machine learning (ML) methods were tested. A 93.4% classification accuracy was reported for distinguishing between three groups: motorcycles, passenger cars and pickups, and heavy trucks. However, more than 90% of the dataset was composed of passenger cars. In [34], an array of MAG and accelerometers sensors was proposed for vehicle detection, speed estimation, and classification. Three MAG nodes positioned longitudinally report vehicle arrivals and departures, and six accelerometers spaced 6-inch apart were positioned over half the lane to detect vehicle axles via a peak detection algorithm. Although the method showed promising results, it was deemed expensive and required an enormous amount of intrusive work and high processing capability. Authors in [38] developed a features selection model for vehicle classification using a single MAG in which 17 features were initially identified and extracted, but only 10 optimal features were eventually selected. A limited dataset of 460 vehicles— mostly small cars—resulted in 92.8% average classification accuracy among four-groups, including buses, small-medium cars, and large trucks.

In each of the aforementioned solutions, a single MAG was used for vehicle detection. Speed was estimated using either one or two MAG; and classification was achieved by employing multiple MAG or accelerometers, or a combination of both. In all cases, a standardized wireless protocol (e.g., IEEE 802.15.4) was used. Nonetheless, in most solutions, it was necessary to embed the sensors into the pavement. Hence, such solutions cannot be used for temporary studies or portable traffic surveillance applications (e.g., work zone safety, roadway design studies, and traffic management in atypical situation, like evacuations). Although a variety of methods were proposed, very limited evaluation was performed over a full range of vehicle classes or speeds considered in our solution. Furthermore, presented results do not reflect actual performance, as testing datasets were limited. Semi-trailer and multi-trailer trucks were highly underrepresented. Additionally, some proposed methods are energy-inefficient and require transmission of big chunks of data to access point for processing. This is a fundamental limitation of WSNs, as they are battery-powered and their network operates in unlicensed spectrum where bandwidth is shared among a vast number of various technologies and devices. Data loss is highly probable as a consequence of unstable wireless link due to either interference or heavy trucks traveling over the detection zone. Other methods rely on an assumption that vehicles of the same class moving at the same speed have almost identical signatures. Such an assumption is misleading for the following reasons: 1) Magnetic length does not represent actual vehicle length; 2) Lateral distance might change for the same type of vehicle; and 3) Magnetic length estimation accuracy depends on the sensor's sampling rate tolerance, which typically has an error rate of ±5% and is sensitive to temperature variation. More importantly, to the best of our knowledge, no study reported detection error types, how to optimize MAG sensors for ideal performance, or consistency of MAG sensors output. Furthermore, limited information is provided in literature on system design, algorithm development, and comprehensive analysis in various realistic scenarios.

III. System Description

The multi-disciplinary, innovative integration of embedded system, WSN, and state-of-the-art sensors—coupled with intelligent algorithms—addresses components composition of the developed platform purposefully designed to support various traffic surveillance studies or applications. The system is primarily composed of *i*VCCS, *i*AP, and a cloud server. Fig. 2 illustrates a conceptual diagram of various system elements.

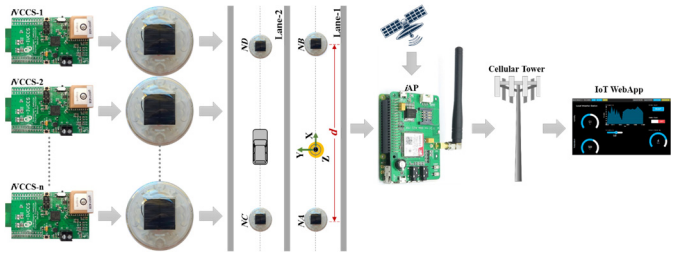

Fig. 2. Conceptual diagram of the developed system

The *i*VCCS are installed into enclosures. Two nodes are deployed in each lane at a distance *d*, and *i*VCCS nodes communicate with an *i*AP over ZigBee wireless network. An

*i*AP connects with a cloud server over a cellular network. The *i*VCCS system block diagram is shown in Fig. 3; the *i*VCCS physical board is illustrated in Fig. 4.

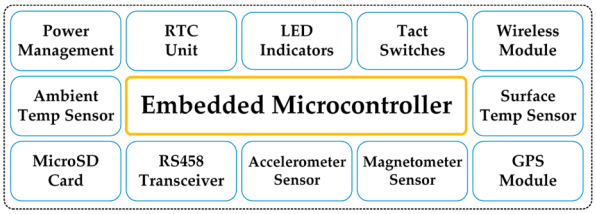

Fig. 3. The *i*VCCS block diagram

*i*VCCS is a battery-powered, smart-sensing node. Its core is an 8-bit pico-power, high-performance microcontroller made by ATMEL—ATxmega128A4. FXOS8700 is a 6-axis MAG and accelerometer. The MAG measures disturbance in the Earth's magnetic field; the accelerometer measures road surface acceleration. FXOS8700 is highly reliable and features a 16-bit ADC resolution and 0.1μT/LSB sensitivity over a dynamic range of ±1200μT.

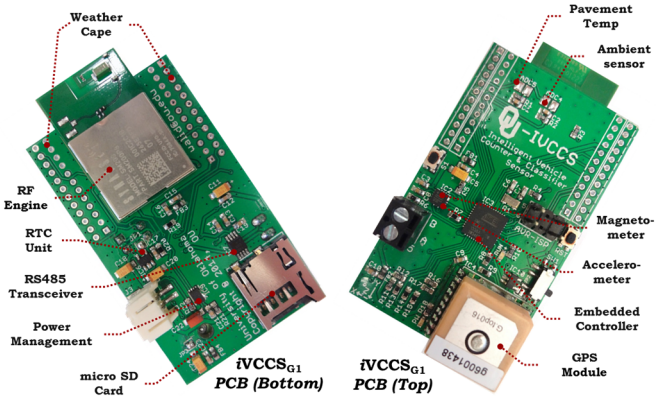

Fig. 4. The *i*VCCS physical board

Highly accurate time-synchronization (T-sync) is enabled by Gms-g6, which is a low power, dual-system, embedded GPS receiver module with built-in patch antenna [39]. Gms-g6 is also used to enable auto-localization and self-organization for a scalable WSN deployment.

The MCU's internal RTC is adaptively calibrated using Gms-g6 and is coupled with highly accurate external crystal for time-stamping of vehicle arrival and departure instants.

The wireless intercommunication between various network devices is facilitated via Synapse SM200P81 RF Engine [40] with Synapse's SNAP [41] on top. SNAP is a mesh network operating system facilitates self-healing, multi-hop, instant-on, and internet-enabled mesh networking over the network. The system is powered by a 3.7V/2000mAh Li-Po battery. Li-Po batteries are a best-fit for powering handheld and portable devices. They are small, lightweight, and durable. However, a deep discharging could render the battery unusable. MAX17043 [42] was added to prevent this. The chip uses sophisticated algorithms to detect battery state, including voltage, current, capacity, alarm, and other datasets. The data acquisition unit facilitates data storage on a micro-SD card. The unit is connected and managed directly by the MCU through a 10Mbps serial peripheral interface (SPI). The micro-SD card supports auto-sleep mode to conserve power. Road surface condition monitoring sensors (i.e., wet/dry and temperature) were added for pavement temperature analysis.

IV. Algorithms Development and Integration

Providing reliable traffic-monitoring data requires precise vehicle detection and highly accurate speed estimation. Precise detection demands a consistent baseline and coherent sampling rate. Speed estimation relies on precise time-stamping of vehicle arrival and departure instants, which is dependent on T-sync algorithm accuracy. In the following section, the development and integration of various distinctive algorithms for real-time traffic surveillance are discussed in detail. Fig. 5 illustrates a block diagram for the relationships among various developed algorithms and associated interconnection with system's hardware interfaces and physical components.

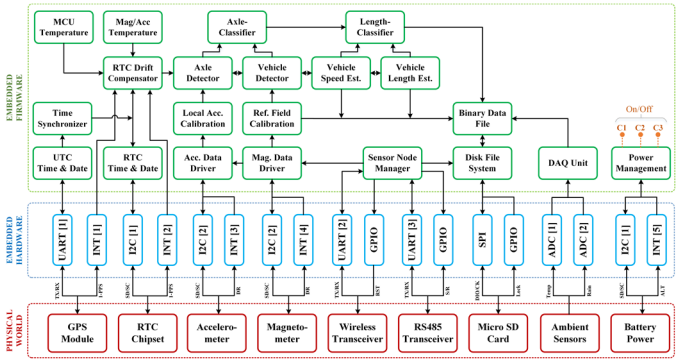

Fig. 5. The integration of hardware and software in the *i*VCCS system

B. Vehicle Detection and Counting

A five-state machine process algorithm was developed for real-time vehicle detection and counting, using a single *i*VCCS node. The algorithm processes the Earth's magnetic field flux magnitude (F_M), which is calculated as the square-root of the three geomagnetic field components (i.e., B_X, B_Y, and B_Z). Localized flux lines are pulled away from the sensor as a vehicle passes the sensor zone and pushed back toward the sensor as the vehicle drives away (see Fig. 1), creating fluctuations in F_M. The five-state machine process analyzes these fluctuations for valid vehicle detection by means of three-adaptive thresholds and three-adaptive debounce-timers, as shown in Fig. 6.

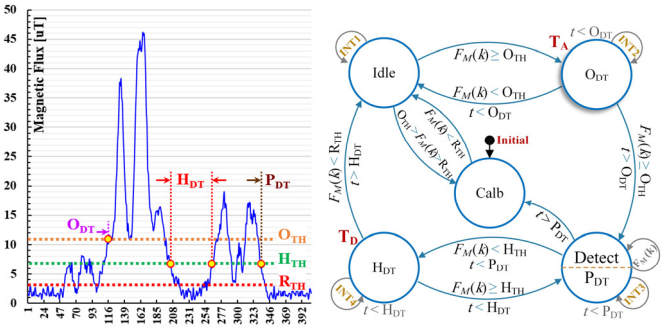

Fig. 6. Vehicle magnetic magnitude (left) - five-state machine process (right)

Upon system power up, an initialization process triggers a *Calibration state* where MAG samples the localized magnetic field for a period T_S in absence of any vehicles. T_S is subject

to the sensor's output data rate (ODR) and number of samples. Ten samples at ODR>100Hz was found sufficient for the calibration process. During this time, the reference magnetic field flux magnitude $F_{Mref}(k)$ is calculated using (1), where $B_{Xref}(k)$, $B_{Yref}(k)$, and $B_{Zref}(k)$ serve as the localized geomagnetic field reference components.

$$F_{Mref}(k) = \sqrt{B_{Xref}(k)^2 + B_{Yref}(k)^2 + B_{Zref}(k)^2} \quad (1)$$

$F_{Mref}(k)$ is normally distributed with a mean μ and standard deviation σ such that $F_{Mref} \propto \mathcal{N}(\mu, \sigma)$. Hence, the *baseline threshold* (R_{TH}) that defines a recalibration is estimated as shown in (2). Consequently, *onset threshold* (O_{TH}), which defines vehicle arrival, and *holdover threshold* (H_{TH}), which defines vehicle departure, are calculated according to (3) and (4), respectively, where α and β are experimentally defined coefficients for an optimal detection (See Section IV.D) and $\alpha > \beta$ provides a hysteresis property in detection. F_{Mref} should unilaterally be adaptively tracked and compensated, as described next in section IV.C.

$$R_{TH} = \mu + 2\times\sigma \quad (2)$$

$$O_{TH} = \mu + \alpha\times\sigma \quad (3)$$

$$H_{TH} = \mu + \beta\times\sigma \quad (4)$$

The node remains in *Idle state* until condition $F_M(k) \geq O_{TH}$ (i.e., vehicle in detection zone) is true; $F_M(k)$ is found in (5).

$$F_M(k) = \sqrt{\left(B_X(k) - B_{Xref}\right)^2 + \left(B_Y(k) - B_{Yref}\right)^2 + \left(B_Z(k) - B_{Zref}\right)^2} \quad (5)$$

To eliminate misdetection errors as a result of a glitch or transient state and to filter out false events, an *onset debounce-timer* (O_{DT}) is used. A transition into *Detect state* occurs if O_{DT} is elapsed and the condition $F_M(k) \geq O_{TH}$ is still true.

To eliminate double-detection errors due to fluctuations in F_M that could possibly occur between O_{TH} and H_{TH} given that part of the vehicle has relatively small magnetic flux density (e.g., long combination trucks), a *holdover debounce-timer* (H_{DT}) is used. H_{DT} plays a significant role in reducing detection errors. A transition from *Detect state* into *H_{DT} state* occurs if $F_M(k) < H_{TH}$ becomes true (i.e., vehicle departed the detection zone). A transition into *Idle state* occurs after H_{DT} is elapsed and $F_M(k) < H_{TH}$ is true. Vehicle counter will then be incremented by one, and vehicle arrival time (T_A) and departure time (T_D) will be logged. A detection period-timer (P_{DT}) is implemented for stationary detection applications.

For detection when *i*VCCS nodes are installed in a roadside setup adjacent to the lane, instead of a roadway setup, in the center of a lane, a moving average filter (MAF) with a gain *w* must be employed to reduce signal fluctuations and increase MAG SNR. $F_{M_{gain}}(k)$ in (6) is the detection algorithm input.

$$F_{M_{gain}}(k) = \frac{w}{N}\sum_{i=0}^{N-1} F_M(k-i); \quad w = 4, \; N = 5 \quad (6)$$

C. Adaptive Compensation of Baseline Drift

Variations in temperature, vibrations, and aging will cause a considerable drift in the mean value of $F_{Mref}(k)$, which causes detection errors. Tracking $F_{Mref}(k)$ is achieved using a MAF when $F_M(k) < O_{TH}$ condition is true. The algorithm computes new B_{Xref}, B_{Yref}, and B_{Zref} values as in (7) if (8) is satisfied. M, the number of samples, was set experimentally equal to 10.

$$B_{ref}^{(\gamma)} = \frac{1}{M}\sum_{i=0}^{M-1} B^{(\gamma)}(k-i); \quad \gamma = \{X, Y, Z\} \in \mathbb{R}^3 \quad (7)$$

$$\frac{1}{M}\sum_{i=0}^{M-1}\left[F_{M_{ref}}(k-i) - F_{M_{ref}}(k)\right] \geq R_{TH} \quad (8)$$

Fig. 7 shows a drift in F_{Mref} over 240 minutes without (in yellow) and with (in blue) the adaptive compensation algorithm. The right figure shows F_{Mref} distribution with compensation (μ=1.79μT, σ=0.7μT) and without (μ=7.67μT, σ=1.6319μT). A high-level description is illustrated in Alg. 1.

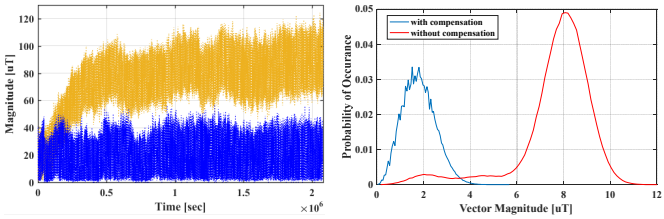

Fig. 7. The drift in F_{Mref} with and without adaptive compensation

Inputs: $B_X(k)$, $B_Y(k)$, $B_Z(k)$
Outputs: B_{Xref}, B_{Yref}, B_{Zref}
WHILE $F_M(k) < O_{TH}$
  WAITFOR Magnetometer *Data-Ready INT*
  BUFFER ← COMPUTE $F_M(k)$ ← READ $B_X(k)$,$B_Y(k)$, $B_Z(k)$
  $Idx \leftarrow Idx + 1$
  IF $Idx = M$ **THEN**
    $F_{M.Avg} \leftarrow \frac{1}{M}\sum_{j=0}^{M-1} F_M[k-j]$
    IF $O_{TH} > F_{M\text{-}Avg} \geq R_{TH}$ **THEN**
      $B_{Xref}, B_{Yref}, B_{Zref} \leftarrow \frac{1}{M}\sum_{i=0}^{M-1} B^{(\gamma)}[k-i]$
    ENDIF
    $Idx \leftarrow 0$: BUFFER ← 0
  ENDIF
LOOP
$Idx \leftarrow 0$: BUFFER ← 0

Alg. 1. Adaptive Baseline Drift Compensation Pseudocode

D. Defining Optimal Detection Thresholds

The F_M measurements of 12,000 vehicles of various FHWA F scheme classes [43] collected using *i*VCCS on highway and urban roads were statistically analyzed to determine the O_{TH}, H_{TH}, and R_{TH} values guarantying best performance.

F_M measurements can be represented as two Gaussians of a single dimension dataset. One Gaussian represents noise, and the other represents vehicle signatures. Since no information is given about which points belong to which distribution, a Gaussian Mixture Model (GMM) is used to separate the two distributions, assuming both are normally distributed.

GMM is a parametric probability density function of continuous measurements represented as a weighted sum of *M* component Gaussian densities (CGD), where *x* is a data vector of *d*-dimensional continuous measurements such that $x = [x^1, x^2, \ldots, x^d]^T$; Σ is the covariance matrix of the Gaussian; *J* is the number of Gaussians; ω_i is the weight of Gaussian *i* such that $\sum_i \omega_i = 1$, $\omega_i \geq 0$, and $\mathcal{N}(x|\mu_i, \Sigma_i)$; and $i = 1 \ldots J$ is the CGD. GMM parameters are estimated from training dataset by maximum likelihood using expectation-maximization.

Since d=1 and J=2, CGD can be rewritten as given in (9) and (10), where x_i is a vector of F_M readings (32,905,300), and μ_n, σ_n^2 and μ_s, σ_s^2 are mean and variance of noise and vehicle signature, respectively.

$$\mathcal{N}(x_i|\mu_s,\sigma_s^2) = \frac{1}{\sqrt{2\pi\sigma_s^2}}\exp\left\{-\frac{(x_i-\mu_s)^2}{2\sigma_s^2}\right\} \quad (9)$$

$$\mathcal{N}(x_i|\mu_n,\sigma_n^2) = \frac{1}{\sqrt{2\pi\sigma_n^2}}\exp\left\{-\frac{(x_i-\mu_n)^2}{2\sigma_n^2}\right\} \quad (10)$$

These can be solved using Bayesian's role by calculating the likelihood to which Gaussian each value of F_M belongs using (11) and (12). The result is two distributions, as shown in Fig. 8, where μ_n=18.6; σ_n=8.24; μ_s=153.5; and σ_s=153.3. By substituting μ_n, σ_n in (2), (3), and (4), and considering β=5 and α=6 (i.e., 6σ represents 99.999% confidence level), we find R_{TH}=35; O_{TH}=68; and H_{TH}=60 are the optimal thresholds. The obtained values are universal and can be used other field deployments.

$$p(\mu_s,\sigma_s^2|x_i) = \frac{p(x_i|\mu_s,\sigma_s^2)p(\mu_s,\sigma_s^2)}{p(x_i|\mu_s,\sigma_s^2)p(\mu_s,\sigma_s^2)+p(x_i|\mu_n,\sigma_n^2)p(\mu_n,\sigma_n^2)} \quad (11)$$

$$p(\mu_n,\sigma_n^2|x_i) = 1 - p(\mu_s,\sigma_s^2|x_i) \quad (12)$$

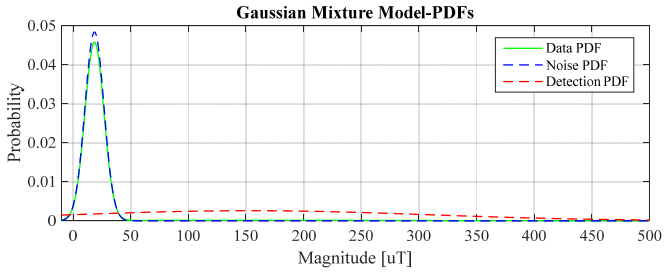

Fig. 8. Distribution of magnetic noise and signature separated using GMM

E. Defining Optimal Values for H_{DT}

Three detection errors can be observed if MAG is used for vehicle detection, namely mis-, double-, and false-detection.

Mis-detection occurs when two vehicles driving at close proximity are grouped as one when the condition $g_T < H_{DT}$ is true (See Fig. 9), where g_T is the gap time between departure of vehicle i and arrival of vehicle $i+1$ at a detection point x.

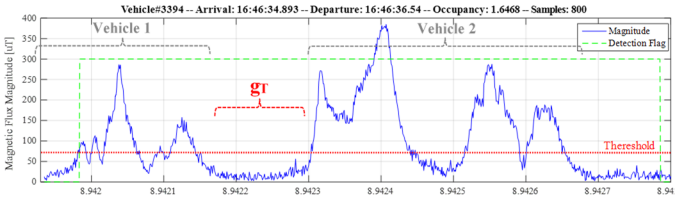

Fig. 9. Miss-detection caused by two vehicle driving at close proximity

Double-detection is observed with combination trucks (See Fig. 10), as their structure can be magnetically divided into three sections: lead, center, and tail. The central section $S^{(2)}$ has a small magnetic flux density, making $F_M(k) < H_{TH}$ true for duration $S^{(2)}_T > H_{DT}$ if truck speed is relatively slow. This phenomenon is referred to in literature as *pulse break-up* [44].

False-detection is typically caused by a vehicle with high magnetic flux density that is passing in the adjacent lane or at the edge of designated lane. This creates a disturbance that will be detected by sensors in both lanes.

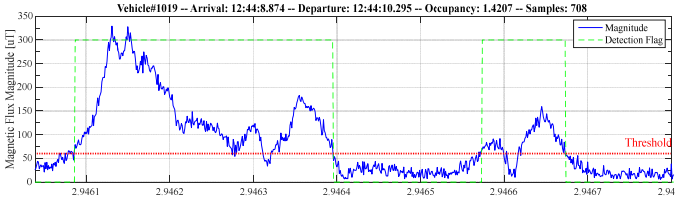

Fig. 10. Double detection caused by class 9 vehicle

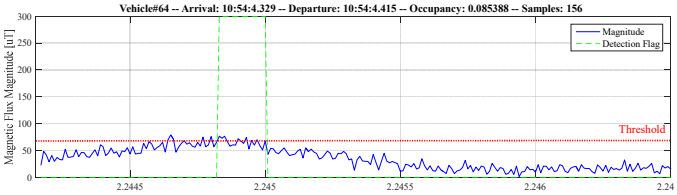

Fig. 11. False detection caused by class 5 vehicle passing in the adjacent lane

To minimize mis- and double-detection errors, H_{DT} value should satisfy the condition $g_T > H_{DT} > S^2_T$.

1) Minimizing miss-detection error

Minimizing mis-detection errors was achieved by statistically analyzing g_T, computed using (13) from data collected using *i*VCCS. The dataset included 13,400 records collected from highway conditions, in addition to 17,180 records collected on urban roads. Probability density function (PDF) and cumulative distribution function (CDF) were subsequently found. CDF showed that setting H_{DT} to 370ms for highway setup and 430ms for urban road setup can reduce mis-detection error to 0.1865% and 0.5065%, respectively.

$$g_T(k) = T_A(k+1) - T_d(k) \quad (13)$$

2) Minimizing double-detection error

PDF and CDF of $S^{(2)}_T$ for 1770 vehicle of class 8, 9, and 10 were found from data collected using *i*VCCS on highway and urban roads for a speed range of 25 to 88mph. The computation process for S^2_T is depicted in Fig. 12. CDF showed that the longest S^2_T is 500ms.

Fig. 12. S^2_T extraction and computation process

The error probability distribution showed a 0.004% and 0.005% probability of double-detection error when setting H_{DT}≥400ms and H_{DT}≥370ms, respectively.

3) Minimizing false-detection error

Changing MAG sensor sensitivity is not a valid approach for minimizing false-detection, as this would cause mis-detecting motorcycles and delayed detection of other vehicles. To solve this issue, variations in B_X, B_Y, and B_Z were analyzed to measure the effect of vehicles on an adjacent lane interfering on each component. Analysis showed insignificant interfering effect on B_Z. Hence, by using 10-tap MAF, calculating $B_Z(k)$ mean, as in (14), and comparing μB_Z for each detected vehicle (V_n) with a threshold I_{TH}, a decision can be made whether V_n is a real detection or an interfering signal. I_{TH} =8μT was statistically found from the dataset.

$$\mu B_Z(V_n) = \frac{1}{N}\sum_{k=1}^{N}\left(\frac{1}{M}\sum_{i=0}^{M-1} B_{Zm}(k-i)\right) \geq I_{TH};\ B_{Zm}(k) = \sqrt{(B_Z(k)-B_{Zref})^2} \quad (14)$$

Obtained H_{DT} and I_{TH} are universal optimal values and can be used in other field deployments.

F. Vehicle Speed Estimation

The most accurate and computationally efficient method to estimate vehicle speed is calculating travel time between two longitudinally positioned nodes ($N_A \rightarrow N_B$) separated by a distance d using (15), as shown in Fig. 13. The following assumptions are made when estimating speed using (15): 1) Sensors A and B are precisely installed at a distance d; 2) No lane changing occurs between sensors A and B.

$$\bar{v}_i \approx \frac{d^{(N_A \rightarrow N_B)}}{T_A^{(N_B)} - T_A^{(N_A)}} \approx \frac{d^{(N_A \rightarrow N_B)}}{T_D^{(N_B)} - T_D^{(N_A)}} \approx 2\frac{d^{(N_A \rightarrow N_B)}}{T_A^{(N_B)} - T_A^{(N_A)} + T_D^{(N_B)} - T_D^{(N_A)}} \quad (15)$$

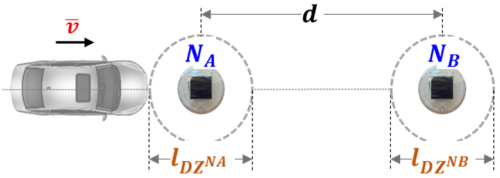

Fig. 13. Speed estimation deployment setup

G. Time Synchronization using GPS

Each sensor node relies on an onboard GPS module and RTC unit to maintain an independent local globally synchronized to the GPS's pulse-pre-second (PPS) signal. Therefore, wireless sync packets are not necessary for accurate functioning of *i*VCCS nodes. A detailed description on the development and implementation of system network architecture, time synchronization, and drift compensation can be reviewed in [45].

H. Vehicle Magnetic Length Estimation

Vehicle magnetic length (VML) is defined as a disturbance in the Earth's magnetic field caused by a vehicle structure. VML is estimated from the product of vehicle speed and sensor occupancy time $T_{Occ}^{(N_i)}$, as in (16). A $T_{Occ}^{(N_i)}$ is defined as the difference between vehicle departure and arrival times at a designated detection point.

$$\overline{VML} = \bar{v} \times T_{Occ}^{(N_i)} = \bar{v} \times \left(T_D^{(N_i)} - T_A^{(N_i)}\right) = \bar{v} \times \frac{T_D^{(N_A)} - T_A^{(N_A)} + T_D^{(N_B)} - T_A^{(N_B)}}{2} \quad (16)$$

Because disturbance level to the Earth's magnetic field depends on vehicle composition of ferrous materials, vehicle magnetic length can theoretically be longer than its actual physical length. Nevertheless, under the assumptions 1) symmetrical detection zone and 2) sensor sensitivity are independent of vehicle structure, vehicle physical length can be estimated as in (17), where l_{DZ} is the estimated length of sensor's detection zone (See Fig. 13).

$$\bar{l}_V = l_M - l_{DZ}^{(Ni)}; \qquad \widehat{l_{DZ}^{(Ni)}} \approx \bar{v}_i \left[T_D^{(N_B)} - T_A^{(N_A)}\right] - d^{N_A \rightarrow N_B} \quad (17)$$

I. Magnetic Length-based Vehicle Classification

Information on vehicle class is crucial for all aspects of a transportation agency's design, planning, safety, analysis, and management. Most traffic engineering and planning processes require information only about car vs. truck volume, as trucks have a major impact on reducing road service life. *The FHWA Traffic Monitoring Guide* [43] provides a length-based vehicle classification (LBVC) based on nationwide IDL data. The proposed scheme bins vehicles into four groups, including passenger vehicles, single-unit trucks, combination trucks, and multi-trailer trucks. Several U.S. states have started defining LBVC boundaries that fit vehicle characteristics, which vary among U.S. states.

Unlike IDL, MAG is a passive sensor. The amount of ferrous materials in a vehicle structure plays a major role in defining detection range. A vehicle with a large amount of steel can be detected from a long distance, making the use of MAG for LBVC challenging. Furthermore, VMS sampled using MAG have an inconsistent peak magnitude and shape parameter; Significant fluctuations in signature and variations in magnetic length can be observed in each vehicles class.

To define boundaries for a real-time LBVC using MAG, several ML classification methods were investigated (e.g., Decision Trees (DT), Support Vector Machine (SVM), *k*-Nearest Neighbor (*k*NN), and Naïve Bayes Classifier (NBC)). All algorithms used a one-vs.-all approach. Predictive accuracy of fitted models was examined using 10-fold cross-validation. Results are reported in the next section.

V. Field Study and Data Analysis

A. Deployments setup

Seven major field tests were conducted—three of which were on highway *U.S. 412, Chouteau, OK 74337 USA,* one on an urban road at *S. Yale Ave., Tulsa, OK 74135 USA,* the fifth test took place at *Lake Hefner Pkwy,* in OKC and the last two deployments were conducted at *536 W State Hwy 152, Mus*tang, OK, and *Will Rogers Expy, OKC, OK*. The data collected from the first four field tests were used for system optimization and data collected in the last three field tests were used for system validation and performance evaluation. Several *i*VCCS nodes were installed on the left lane center of *roadway surfaces* and adjacent to the left lane of *roadsides surfaces*. All nodes were positioned with x-axis along traffic direction; y-axis perpendicular to traffic; and z-axis perpendicular to the ground, pointing upward. All nodes were operated by *i*APs installed on the road shoulder. Video camera and *Road Runner 3 Kit* [46] from Diamond Traffic were used as ground-truth. Cameras, *Road Runner kit*, *i*VCCS nodes, and *i*APs were synchronized using a GPS-based clock. Vehicles classes were manually extracted from video images by counting the number of axles for each vehicle. Measured speed was calculated using *Road Runner kit* to validate estimated speed by *i*VCCS. Deployment setup for the first three test is shown in Fig. 14.

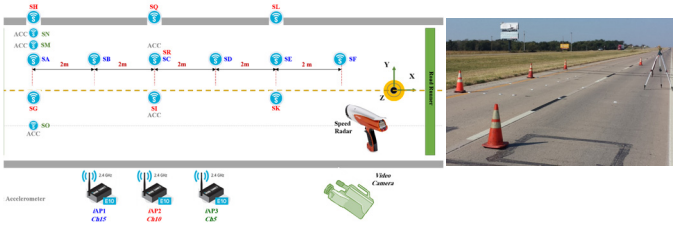

Fig. 14. Highway deployment setup layout on roadway and roadsides

B. Vehicle Detection and Counting Accuracy

Counting accuracy was evaluated using the mean absolute percent error (MAPE) in (18). Roadway setup in the first four tests showed 99.65% detection accuracy for both highway and urban road tests (See TABLE I). A mis-detection error was observed in class 2 when two vehicles were driving on a highway at 88mph within close proximity. As a result, their magnetic signatures were combined. Double-detection errors were observed in class 9 on the urban road test when trucks measuring 23-meters were driving at 20mph.

$$MAPE = \frac{1}{n}\sum_{1}^{n}\frac{|\text{Count}_{\text{video}} - \text{Count}_{i\text{VCCS}}|}{|\text{Count}_{\text{video}}|}\times 100 \quad (18)$$

TABLE I
VEHICLES DETECTION AND COUNTING ACCURACY – ROADWAY SETUP

Vehicle Class	Video Count	*i*VCCS Count	MAPE
F01	22	22	0
F02	6949	6947	0.028
F03	3989	3989	0
F04	16	16	0
F05	358	358	0
F06	92	92	0
F07	1	1	0
F08	28	28	0
F09	621	623	0.322
F10	9	9	0
Total	**12085**	**12085**	**0.35%**

In an offline analysis, 113 false-detection errors were caused by interference from an adjacent lane. Also, in the urban road test, 38 class 2 and class 3 vehicles were detected by sensors in both lanes when they were driven in-between the two lanes. Such errors are not reflected in TABLE I. The counting accuracy for all tests is presented in TABLE II.

TABLE II
VEHICLES DETECTION AND COUNTING ACCURACY – ALL TESTS

Vehicle Class	Video Count	*i*VCCS Count	MAPE
Test 1	463	470	1.5%
Test 2	2007	2005	0.099%
Test 3	2754	2753	0.036%
Test 4	6861	6976	1.676%
Test 5	3997	3984	0.40705%
Test 6	828	815	1.57%
Test 7	1252	1260	0.639%

A roadside-setup test confirmed 99.95% detection accuracy. Variations in flux magnitude in roadside scenarios are relatively uniform when compared to roadway, which accounts for slightly better accuracy. However, roadside setup is not applicable for a road with more than two lanes.

C. Stationary Detection in Roadway and Roadside Setups

The same algorithm was tested for stop-go scenarios (e.g., at traffic signals and intersections and static state scenarios (e.g., parking lot and garage door). Obtained detection accuracy was 100% in both roadside- and roadway-setup scenarios. Fig. 15 shows the F_M for a go-stop-go scenario in both roadside and roadway setups. G_A, S_S, and G_D represent vehicle arrival section (Go-in), vehicle in steady state (Stop); and vehicle departure section (Go-out).

The value of P_{DT} must be configured according to intended application. Moreover, P_{DT} value in stationary detection can be used as a timer for parking duration.

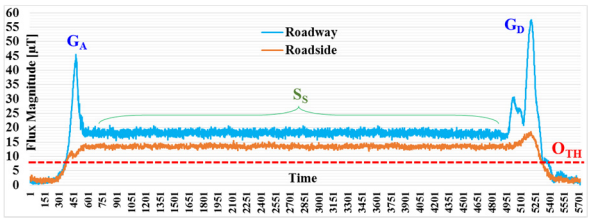

Fig. 15. The F_M and detection flag in Go-Stop-Go scenario

D. Vehicle Speed Estimation Accuracy

Speed accuracy was evaluated against *Road Runner 3 kit* using a 30.5μs event timestamp resolution [46]. Two statistical measurements were used—MAPE, which measures systematic bias to error such that estimated speed values are consistently high or low (19), and Root Mean Square Error (RMSE), which measures mean deviation of estimated speed values (20). Speed analysis is shown in TABLE III.

Three separations between the nodes, namely 6-, 8-, and 10meter, where investigated. Separating two nodes by 8 meters was found superior. Roadside setup showed a higher speed estimation error when compared to roadway setup. This can be explained by a lower SNR in the roadside scenario.

$$MAPE = \frac{1}{n}\sum_{i=1}^{n}\left|\frac{True\ Speed_{(i)} - Estimated\ Speed_{(i)}}{True\ Speed_{(i)}}\right|\times 100 \quad (19)$$

$$RMSE = \sqrt{\frac{1}{n}\sum_{i=1}^{n}\left(True\ Speed_{(i)} - Estimated\ Speed_{(i)}\right)^2} \quad (20)$$

TABLE III
VEHICLES DETECTION AND COUNTING ACCURACY – ROADWAY SETUP

Setup	RMSE	MAPE	Accuracy
Roadside (*d*=6m)	6.4603 mph	6.5001%	93.5012%
Roadway (*d*=6m)	3.2064 mph	2.6585%	97.3415%
Roadway (*d*=8m)	2.9281 mph	2.5773%	97.4227%
Roadway (*d*=10m)	2.9867 mph	2.5218%	97.4782%

E. Vehicle Magnetic Length Estimation

The per-class histograms of VML estimated using (16) is shown in Fig. 16. Statistical measurements are presented in TABLE IV. An overlap between class 2 and class 3, classes 4 through 7, and classes 8 through 10 were observed. Classes 11 through 13 were not observed during the tests. Significant variation in VML per class is attributed to differences in the amount of permeable ferrous materials in per vehicle structure.

F. Magnetic LBVC Accuracy

By analyzing VML distributions presented in Fig. 16 and their statistical measurements in TABLE IV, several LBVC schemes, namely three-, four-, and five-group, were developed and evaluated by means of ML. The objective of the five-group scheme is providing a distinction between Motorcycles (MC), Passenger Vehicles (PV), Single-Unit Trucks (SU), Semi-trailer (ST) Trucks, and Multi-trailer (MT) Trucks. MT vehicles, i.e., F11-F13, are missing in the dataset. Thus, the four-group LBVC scheme (See TABLE V), which lumps ST and MT in one group, will be reported in this work.

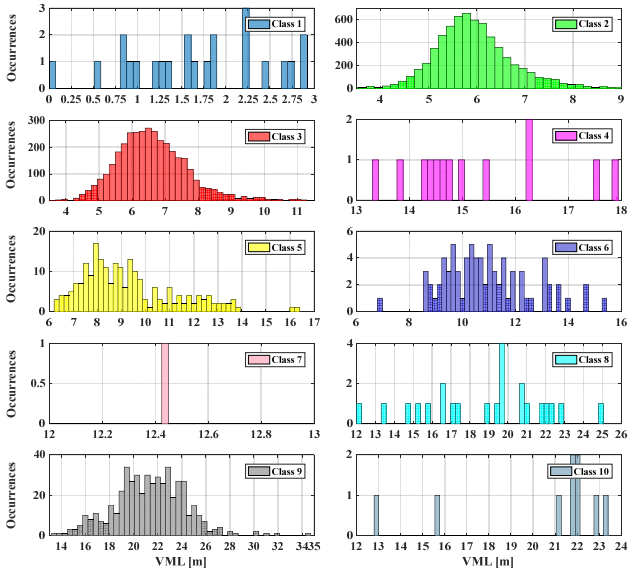

Fig. 16. Histograms of VML by FHWA Scheme F – Classes 1 to 10

TABLE IV
VML STATISTICAL MEASUREMENTS FOR FHWA SCHEME F

Class	Mean	STD	VAR	Max	Min
F01	1.7629	0.7156	0.5120	2.9106	0.5370
F02	5.9383	0.8190	0.6708	11.0377	2.7606
F03	6.6140	1.0713	1.1477	12.5161	3.5516
F04	15.2446	1.3782	1.8996	17.9241	13.3784
F05	9.2552	1.9270	3.7132	16.3884	6.2894
F06	10.9073	1.6149	2.6078	15.4366	6.8855
F07	12.4458	0	0	12.4458	12.4458
F08	18.8185	3.2396	10.4950	25.0102	12.0606
F09	21.3425	2.9298	8.5840	34.6607	13.5164
F10	20.3949	3.5930	12.9097	23.3700	12.9307

TABLE V
VML STATISTICAL MEASUREMENTS FOR FOUR-GROUP SCHEME

Class	Mean	STD	VAR	Max	Min
G1	1.6863	0.7899	0.6239	2.9106	0.5370
G2	6.1783	0.9720	0.9447	12.5161	2.7606
G3	9.7024	1.9890	3.9561	16.3884	6.2894
G4	21.0714	3.1055	9.6439	34.6607	12.0606

Ten commonly-used performance metrics were selected to evaluate classifier performance (i.e., classification rate (C_R), MAPE, RMSE, true positive rate (TPR), false positive rate (FPR), F-measure (F1), Matthews's correlation coefficient (MCC), and the area under ROC curve (AUC)). TABLE VI illustrates that all classification methods showed comparable high performance in assigning vehicles to the correct class.

TABLE VI
VML STATISTICAL MEASUREMENTS FOR FHWA SCHEME F SCHEME

		Classification Method			
Criteria		**DT**	***k*-NN**	**C-SVM**	**NBC**
Average	**C_R**	97.65%	97.76%	97.83%	97.58%
	MAE	0.021	0.016	0.010	0.016
	RMSE	0.105	0.096	0.104	0.100
Weighted Average	**TPR**	0.977	0.978	0.978	0.976
	FPR	0.235	0.202	0.208	0.143
	Precision	0.972	0.974	0.975	0.976
	Recall	0.977	0.978	0.978	0.976
	F1	0.971	0.974	0.974	0.976
	MCC	0.835	0.843	0.848	0.839
	AUC	0.882	0.960	0.885	0.987

A decision tree model was adopted primarily because it is easy to implement and it is memory efficient. Optimal values for parameters in the aforementioned ML classification methods were found using hyper-parameter optimization algorithms. A probabilistic modeling can also be used to identify decision boundaries among classes [48].

G. Sensor's Output Consistency

Evaluating consistency of VMS sampled using several sensors under similar test conditions is crucial for vehicle classification and re-identification applications. The statistical relationship between sampled VMS from first four aligned sensors (i.e., S_A, S_B, S_C, and S_D) in Fig. 14 was found by means of cross-correlation data analysis.

A correlation coefficient R was used to express correlation strength between signals. Pearson's correlation coefficient is the most common measure of linear dependence between two random variables, A and B, as defined in (21). A μ_A and σ_A are mean and STD of A, and μ_B and σ_B are mean and STD of B.

$$\rho(A,B) = \frac{cov(A,B)}{\sigma_A \sigma_B} = \frac{1}{N-1}\sum_{i=1}^{N}\frac{(A_i-\mu_A)(B_i-\mu_B)}{\sigma_A \sigma_B} \tag{21}$$

Given that our investigation had four sensors, R for pairwise signals was first found using (21), and then the correlation coefficient matrix for all signals was found by combining the Rs of all pairwise variable, as in (22). Diagonal entries are always equal to 1, as all signals are directly correlated to themselves.

$$MR = \begin{pmatrix} 1 & \rho(F_M^{(N_A)},F_M^{(N_B)}) & \rho(F_M^{(N_A)},F_M^{(N_C)}) & \rho(F_M^{(N_A)},F_M^{(N_D)}) \\ \rho(F_M^{(N_B)},F_M^{(N_A)}) & 1 & \rho(F_M^{(N_B)},F_M^{(N_C)}) & \rho(F_M^{(N_B)},F_M^{(N_D)}) \\ \rho(F_M^{(N_C)},F_M^{(N_A)}) & \rho(F_M^{(N_C)},F_M^{(N_B)}) & 1 & \rho(F_M^{(N_C)},F_M^{(N_D)}) \\ \rho(F_M^{(N_D)},F_M^{(N_A)}) & \rho(F_M^{(N_D)},F_M^{(N_B)}) & \rho(F_M^{(N_D)},F_M^{(N_C)}) & 1 \end{pmatrix} \tag{22}$$

CDF for all pairwise combinations revealed that most values of R are between 0.9 and 1, indicating high similarity in sensor output across multiple nodes. Furthermore, the p-value matrix returned very small p-values (i.e., 2e-138), which reject the null hypothesis and identify significant correlations.

VI. CONCLUSION

This study reported the design and development of a novel, intelligent vehicle counting and classification system (*i*VCCS) that uses wireless magnetometer sensor for real-time traffic surveillance. Reliable and computationally efficient intelligent algorithms for vehicle detection, speed and length estimation, LBVC, and baseline drift compensation were fully developed, integrated, and evaluated. Investigations revealed consistent and accurate performance under both free flow and congested traffic on highway and urban roadway conditions. A 99.65%, 99.95%, 97.42%, and 97.65% accuracy was reported for roadway detection, roadside detection, speed estimation, and LBVC, respectively. The developed platform is portable and cost-effective—a single sensor node costs approximately $40. It can be used for short-term installment (e.g., work zone safety, traffic flow studies, roadways and bridges design, traffic management in atypical situations), as well as long-term deployment (e.g., collision avoidance at intersections, traffic monitoring, etc.) on surface of roadways and roadsides.

VII. ACKNOWLEDGMENT

The authors would like to acknowledge Oklahoma Department of Transportation (ODOT) for funding provided to support the research activities of this project.

REFERENCES

[1] "FHWA Forecasts of Vehicle Miles Traveled (VMT): May 2014," *Office of Highway Policy Information*, 2014. [Online]. Available: http://www.fhwa.dot.gov/policyinformation/tables/vmt/vmt_forecast_sum.cfm

[2] "WHO | Global status report on road safety 2015."

[3] "National Highway Traffic Safety Administration (NHTSA), 2013 Traffic Safety Facts FARS/GES Annual Report." [Online]. Available: http://www-nrd.nhtsa.dot.gov/Pubs/812139.pdf.

[4] National Highway Traffic Safety Adminstriation, "The Economic and Societal Impact Of Motor Vehicle Crashes, 2010," Washington, DC, 2014.

[5] "2015 Urban Mobility Scorecard and Appendices — Urban Mobility Information." Available: http://mobility.tamu.edu/ums/report/.

[6] C. C. D. US EPA, "Carbon Dioxide Emissions." [Online]. Available: http://www.epa.gov/climatechange/ghgemissions/gases/co2.html.

[7] L. E. Y. Mimbela and L. a Klein, "A Summary of Vehicle Detection and Surveillance Technologies used in Intelligent Transportation Systems."

[8] S. Cheung, "Traffic Surveillance by Wireless Sensor Networks : Final Report," 2007.

[9] G. Orosz, R. E. Wilson, and G. Stépán, "Traffic jams: dynamics and control.," *Philos. Trans. A. Math. Phys. Eng. Sci.*, vol. 368, no. 1928, pp. 4455–79, Oct. 2010.

[10] A. Haoui, R. Kavaler, and P. Varaiya, "Wireless magnetic sensors for traffic surveillance," *Transp. Res. Part C Emerg. Technol.*, vol. 16, no. 3, pp. 294–306, Jun. 2008.

[11] F. Losilla, A.-J. Garcia-Sanchez, F. Garcia-Sanchez, J. Garcia-Haro, and Z. J. Haas, "A Comprehensive approach to WSN-based ITS applications: a survey.," *Sensors (Basel).*, vol. 11, no. 11, pp. 10220–65, Jan. 2011.

[12] K. Liu, H. Xiong, and H. He, "New method for detecting traffic information based on anisotropic magnetoresistive technology," in *Proc. SPIE 8783, Fifth International Conference on Machine Vision (ICMV 2012): Computer Vision, Image Analysis and Processing*, 2013.

[13] J. L. J. Lan and Y. S. Y. Shi, "Vehicle detection and recognition based on a MEMS magnetic sensor," *2009 4th IEEE Int. Conf. Nano/Micro Eng. Mol. Syst.*, pp. 404–408, 2009.

[14] A. Kaadan and H. H. Refai, "iICAS: Intelligent intersection collision avoidance system," in *2012 15th International IEEE Conference on Intelligent Transportation Systems*, 2012, pp. 1184–1190.

[15] W. Balid, H. Tafish, and H. H. Refai, "Development of Portable Wireless Sensor Network System For Real-time Traffic Surveillance," in *18th IEEE International Conference on Intelligent Transportation Systems, IEEE - ITSC 2015, September 15-18, 2015*, 2015.

[16] A. Daubaras and M. Zilys, "Vehicle Detection based on Magneto-Resistive Magnetic Field Sensor," *Electron. Electr. Eng.*, vol. 118, no. 2, pp. 27–32, Feb. 2012.

[17] Z. Zhang, X. Li, H. Yuan, and F. Yu, "A Street Parking System Using Wireless Sensor Networks," vol. 2013, no. c, 2013.

[18] H. Zhu and F. Yu, "A Vehicle Parking Detection Method Based on Correlation of Magnetic Signals," vol. 2015, 2015.

[19] S. Taghvaeeyan and R. Rajamani, "Portable roadside sensors for vehicle counting, classification, and speed measurement," *IEEE Trans. Intell. Transp. Syst.*, vol. 15, no. 1, pp. 73–83, 2014.

[20] B. Koszteczky and G. Simon, "Magnetic-based vehicle detection with sensor networks," in *2013 IEEE International Instrumentation and Measurement Technology Conference (I2MTC)*, 2013, pp. 265–270.

[21] W. Zhang, G. Tan, and N. Ding, "Vehicle Speed Estimation Based on Sensor Networks and Signal Correlation Measurement," pp.1–12, 2014.

[22] D.-H. Kim, K.-H. Choi, K.-J. Li, and Y.-S. Lee, "Performance of vehicle speed estimation using wireless sensor networks: a region-based approach," *J. Supercomput.*, vol. 71, no. 6, pp. 2101–2120, 2015.

[23] D. Obertov, V. Bardov, and B. Andrievsky, "Vehicle speed estimation using roadside sensors," in *2014 6th International Congress on Ultra Modern Telecommunications and Control Systems and Workshops (ICUMT)*, 2014, pp. 111–117.

[24] D. Nan, T. Guozhen, M. Honglian, L. Mingwen, and S. Yao, "Low-power Vehicle Speed Estimation Algorithm based on WSN," in *2008 11th International IEEE Conference on Intelligent Transportation Systems*, 2008, pp. 1015–1020.

[25] L. Zhang, R. Wang, and L. Cui, "Real-time traffic monitoring with magnetic sensor networks," *J. Inf. Sci. Eng.*, vol. 27, no. 4, pp. 1473–1486, 2011.

[26] X. DENG, Z. HU, P. ZHANG, and J. GUO, "Vehicle Class Composition Identification Based Mean Speed Estimation Algorithm Using Single Magnetic Sensor," *J. Transp. Syst. Eng. Inf. Technol.*, vol. 10, no. 5, pp. 35–39, Oct. 2010.

[27] H. Li, H. Dong, L. Jia, D. Xu, and Y. Qin, "Some practical vehicle speed estimation methods by a single traffic magnetic sensor," in *2011 14th International IEEE Conference on Intelligent Transportation Systems (ITSC)*, 2011, pp. 1566–1573.

[28] W. Balid, H. Tafish, and H. H. Refai, "Versatile Real-Time Traffic Monitoring System Using Wireless Smart Sensors Networks," in *IEEE Wireless Communications and Networking Conference (WCNC), Track 4 - Services, Applications, and Business,*.

[29] J. Lan, Y. Xiang, L. Wang, and Y. Shi, "Vehicle detection and classification by measuring and processing magnetic signal," *Measurement*, vol. 44, no. 1, pp. 174–180, Jan. 2011.

[30] W. Zhang, G. Z. Tan, H. M. Shi, and M. W. Lin, "A distributed threshold algorithm for vehicle classification based on binary proximity sensors and intelligent neuron classifier," *J. Inf. Sci. Eng.*, vol. 26, no. 3, pp. 769–783, 2010.

[31] B. Yang and Y. Lei, "Vehicle Detection and Classification for Low-Speed Congested Traffic With Anisotropic Magnetoresistive Sensor," *IEEE Sens. J.*, vol. 15, no. 2, 2015.

[32] E.-H. N. E.-H. Ng, S.-L. T. S.-L. Tan, and J. G. Guzman, "Road traffic monitoring using a wireless vehicle sensor network," *2008 Int. Symp. Intell. Signal Process. Commun. Syst.*, 2009.

[33] D. Kleyko, R. Hostettler, W. Birk, and E. Osipov, "Comparison of Machine Learning Techniques for Vehicle Classification Using Road Side Sensors," *2015 IEEE 18th Int. Conf. Intell. Transp. Syst.*, pp. 572–577, 2015.

[34] W. Ma, D. Xing, A. McKee, R. Bajwa, C. Flores, S. Member, B. Fuller, P. Varaiya, S. Member, B. Fuller, P. Varaiya, C. Author, D. Xing, A. McKee, R. Bajwa, C. Flores, and B. Fuller, "A wireless accelerometer-based automatic vehicle classification prototype system," *IEEE Trans. Intell. Transp. Syst.*, vol. 15, no. 1, pp. 1–8, 2014.

[35] S. Networks, "VSN240 Wireless Flush Mount Sensor." [Online]. Available: http://www.sensysnetworks.com/products/sensor/.

[36] N. Wahlstrom, R. Hostettler, F. Gustafsson, W. Birk, N. Wahlström, S. Member, R. Hostettler, F. Gustafsson, W. Birk, N. Wahlstrom, R. Hostettler, F. Gustafsson, and W. Birk, "Classification of driving direction in traffic surveillance using magnetometers," *IEEE Trans. Intell. Transp. Syst.*, vol. 15, no. 4, pp. 1405–1418, 2014.

[37] D. Liu, X. Xu, C. Fei, W. Zhu, X. Liu, G. Yu, and G. Fang, "Direction identification of a moving ferromagnetic object by magnetic anomaly," *Sensors Actuators A Phys.*, vol. 229, pp. 147–153, 2015.

[38] Y. He, Y. Du, L. Sun, and Y. Wang, "Improved waveform-feature-based vehicle classification using a single-point magnetic sensor," *J. Adv. Transp.*, vol. 49, no. 5, pp. 663–682, Aug. 2015.

[39] "GlobalTop Technology Inc. - Titan 2 (GMS-G6)." http://www.gtop-tech.com/en/product/Titan-2-GMS-G6/GPS_Modules_Gms-g6.html.

[40] "Synapse SM200P81 RF Engine." [Online]. https://www.synapse-wireless.com/documents/products/Synapse-SM200P81-Engine-Product-Brief.pdf.

[41] "Synapse's SNAP Network Operating System," *David Ewing*. [Online]. http://synapse-wireless.com/documents/white_paper/Synapse-SNAP-OS-White-Paper.pdf

[42] "Maxim Integrated-MAX17043 Compact, Low-Cost 1S Fuel Gauges." http://www.maximintegrated.com/en/products/power/battery-management/MAX17043.html

[43] F. H. Administration, "Traffic Monitoring Guide," 2013.

[44] H. Lee and B. Coifman, "Identifying and Correcting Pulse-Breakup Errors from Freeway Loop Detectors," *Transp. Res. Rec. J. Transp. Res. Board*, vol. 2256, pp. 68–78, 2011.

[45] W. Balid, "Fully-Autonomous Self-Powered Intelligent Wireless Sensor for Real-Time Traffic Surveillance in Smart Cities," Ph.D. dissertation, Electrical and Computer Engineering Dept., University of Oklahoma, 2016, https://shareok.org/handle/11244/51828.

[46] "Road Runner 3 Counter and Classifier Kit | Diamond Traffic." [Online]. http://diamondtraffic.com/product/RoadRunner3Kit.

Walid Balid, PhD received PhD degree in Electrical & Computer Engineering from the University of Oklahoma in 2016, the B.S. and M.Sc. degrees in Electronic Engineering from University of Aleppo in 2006 and 2011. Currently, he is principal research engineer at Panduit Corp. R&D. Between 2006 and 2012, he worked as senior electronics engineer and later R&D manager at AL-AWAIL Co. In 2013, he was a senior research associate with Qatar University. His research interests include embedded systems, intelligent transportation systems, wireless sensors, industrial electronics, and wireless coexistence.

Hasan Tafish received MSc degree in Electrical & Computer Engineering from the University of Oklahoma in 2015, the BSc. degree in electrical engineering from Damascus University in 2012. Currently he is research engineer at Honda R&D R&D Americas, Inc. His research interests include, digital signal processing, machine learning, deep neural networks, and FPGA based DSP.

Hazem H. Refai, PhD is the Williams Professor for Telecommunication and Networking at the OU School of electrical and computer engineering (ECE). Dr. Refai's current transportation research and development efforts focus on wireless sensor networks for vehicle detection, road surface condition evaluation, and auto-collision avoidance. Previously he investigated medium access control for vehicle-to-vehicle communication and developed portable weigh-in-motion systems and a multi-element piezoelectric sensor for the Oklahoma Department of Transportation. Dr. Refai has published more than 160 refereed papers for national and international conferences and journal articles.